CHEMISTRY OF MATERIALS
Article

Chem. Mater. **2010,** *22,* 2233–2238 2233
DOI:10.1021/cm902681d

Comprehensive Study of Melt Infiltration for the Synthesis of $NaAlH_4$/C Nanocomposites

Philipp Adelhelm,[†] Jinbao Gao,[†] Margriet H. W. Verkuijlen,[‡] Carine Rongeat,[§] Monika Herrich,[§] P. Jan M. van Bentum,[‡] Oliver Gutfleisch,[§] Arno P. M. Kentgens,[‡] Krijn P. de Jong,[†] and Petra E. de Jongh*,[†]

[†]*Inorganic Chemistry and Catalysis, Debye Institute for Nanomaterials Science, Utrecht University, 3584 CA Utrecht, The Netherlands,* [‡]*Physical Chemistry/Solid State NMR, Radboud University, 6525 ED Nijmegen, The Netherlands, and* [§]*IFW Dresden, Institute for Metallic Materials, P.O. Box 270116, D-01171 Dresden, Germany*

Received August 31, 2009. Revised Manuscript Received December 22, 2009

In the search for suitable solid state hydrogen storage systems, $NaAlH_4$ (7.4 wt % H_2) holds great promise due to its suitable thermodynamical properties. However, hydrogen release and uptake are hampered by high activation energies, most likely due to solid state mass transfer limitations. A recent strategy to improve the hydrogen de- and rehydrogenation properties of $NaAlH_4$ is to reduce the particle size to the nanometer scale. We prepared high loadings of nanosized $NaAlH_4$ confined in the pores of a carbon support by melt infiltration. XRD, nitrogen physisorption, high pressure DSC and solid-state NMR are used to evidence that the molten $NaAlH_4$ infiltrates the carbon support, and forms a nanosized $NaAlH_4$ phase lacking long-range order. The confined $NaAlH_4$ shows enhanced hydrogen dehydrogenation properties and rehydrogenation under mild conditions that is attributed to the nanosize and close contact to the carbon matrix.

Introduction

Sodium Alanate ($NaAlH_4$) is an important candidate for the solid-state storage of hydrogen as it is one of the few (complex) metal hydride systems with thermodynamic properties that allow operation at PEM fuel cell working temperatures.[1] However, the decomposition of $NaAlH_4$ is kinetically hindered and decomposition below its melting point (T_m = 181 °C) is very slow.[2,3] An important step forward was the discovery of Ti species as effective catalysts that allowed (partial) reversibility and dehydrogenation at reduced temperatures.[2] More recently, it was found that the addition of carbon additives also leads to lower dehydrogenation temperatures.[4−10] The underlying mechanism is not well understood, but it is suggested that a catalytic effect of carbon might be related to weakening of the Al−H bonds in $NaAlH_4$ because of interaction with the electronegative support.[11]

An alternative approach to improve the de- and rehydrogenation properties of metal hydrides is by decreasing the crystallite size by supporting on a high surface area material using solution impregnation techniques[12−15] or via melt infiltration.[10,16−20] The limited reversibility of the $NaAlH_4$ system is usually attributed to long solid state diffusion paths, due to macroscopic phase segregation upon dehydrogenation.[21]

*Corresponding author. E-mail: P.E.deJongh@uu.nl.

(1) Felderhoff, M.; Weidenthaler, C.; von Helmolt, R.; Eberle, U. *Phys. Chem. Chem. Phys.* **2007**, *9*, 2643–2653.
(2) Bogdanović, B.; Schwickardi, M. *J. Alloys Compd.* **1997**, *253*, 1–9.
(3) Majzoub, E. H.; McCarty, K. F.; Ozolins, V. *Phys. Rev. B* **2005**, *71*, 024118.
(4) Zaluska, A.; Zaluski, L.; Strom-Olsen, J. O. *J. Alloys Compd.* **2000**, *298*, 125–134.
(5) Gross, K. J.; Thomas, G. J.; Jensen, C. M. *J. Alloys Compd.* **2002**, *330−332*, 683–690.
(6) Wang, J.; Ebner, A. D.; Prozorov, T.; Zidan, R.; Ritter, J. A. *J. Alloys Compd.* **2005**, *395*, 252–262.
(7) Pukazhselvan, D.; Gupta, B. K.; Srivastava, A.; Srivastava, O. N. *J. Alloys Compd.* **2005**, *403*, 312–317.
(8) Dehouche, Z.; Lafi, L.; Grimard, N.; Goyette, J.; Chahine, R. *Nanotechnology* **2005**, *16*, 402–409.
(9) Cento, C.; Gislon, P.; Bilgili, M.; Masci, A.; Zheng, Q.; Prosini, P. P. *J. Alloys Compd.* **2007**, *437*, 360–366.
(10) Adelhelm, P.; de Jong, K. P.; de Jongh, P. E. *Chem. Comm.* **2009**, *41*, 6261–6263.
(11) Berseth, P. A.; Harter, A. G.; Zidan, R.; Blomqvist, A.; Araujo, C. M.; Scheicher, R. H.; Ahuja, R.; Jena, P. *Nano Lett.* **2009**, *9*, 1501–1505.
(12) Gutowska, A.; Li, L. Y.; Shin, Y. S.; Wang, C. M. M.; Li, X. H. S.; Linehan, J. C.; Smith, R. S.; Kay, B. D.; Schmid, B.; Shaw, W.; Gutowski, M.; Autrey, T. *Angew. Chem., Int. Ed.* **2005**, *44*, 3578–3582.
(13) Baldé, C. P.; Hereijgers, B. P. C.; Bitter, J. H.; de Jong, K. P. *Angew. Chem., Int. Ed.* **2006**, *45*, 3501–3503.
(14) Baldé, C. P.; Hereijgers, B. P. C.; Bitter, J. H.; de Jong, K. P. *J. Am. Chem. Soc.* **2008**, *130*, 6761–6765.
(15) Zheng, S. Y.; Fang, F.; Zhou, G. Y.; Chen, G. R.; Ouyang, L. Z.; Zhu, M.; Sun, D. L. *Chem. Mater.* **2008**, *20*, 3954–3958.
(16) (a) de Jongh, P. E.; Wagemans, R. W. P.; Eggenhuisen, T. M.; Dauvillier, B. S.; Radstake, P. B.; Meeldijk, J. D.; Geus, J. W.; de Jong, K. P. *Chem. Mater.* **2007**, *19*, 6052–6057. (b) Bogerd, R.; Adelhelm, P.; Meeldijk, J. H.; de Jong, K. P.; de Jongh, P. E. *Nanotechnology* **2009**, *20*, 204019.
(17) Gross, A. F.; Vajo, J. J.; Van Atta, S. L.; Olson, G. L. *J. Phys. Chem. C* **2008**, *112*, 5651–5657.
(18) Wu, H.; Zhou, W.; Wang, K.; Udovic, T. J.; Rush, J. J.; Yildrim, T.; Benderksy, L. A.; Gross, A. F.; Van Atta, S. L.; Vajo, J. J.; Pinkerton, F. E.; Meyer, M. S. *Nanotechnology* **2009**, *20*, 204002.
(19) Gross, A. F.; Ahn, C. C.; Van Atta, S. L.; Liu, P.; Vajo, J. J. *Nanotechnology* **2009**, *20*, 204005.
(20) Stephens, R. D.; Gross, A. F.; Van Atta, S. L.; Vajo, J. J.; Pinkerton, F. E. *Nanotechnology* **2009**, *20*, 204018.
(21) Singh, S.; Eijt, S. W. H.; Huot, J.; Kockelmann, W. A.; Wagemaker, M.; Mulder, F. M. *Acta Mater.* **2007**, *55*, 5549–5557.

Published on Web 02/25/2010

It is believed that this phase segregation can be limited by using $NaAlH_4$ that is nanosized and confined by a support. In this context, improvement was recently reported for a crystalline $NaAlH_4$/C nanocomposite (formed by melt infiltration of carbon aerogels with pore size ~13 nm)[20] and $NaAlH_4$ nanoparticles supported on SiO_2.[15] However, in both cases no detailed information on the nanostructure of the resulting materials was given.

Here we report the synthesis and detailed structural characterization of nanosized $NaAlH_4$ confined in the pores of a carbon material. The material is prepared by melt infiltration of a porous carbon with relatively small pores (mainly 2−3 nm). The melt infiltration and pore filling process were followed using high-pressure differential scanning calorimetry (HP-DSC) and N_2 physisorption measurements. We present a microstructural characterization, combining XRD, N_2 physisorption, and solid-state NMR results, demonstrating that the $NaAlH_4$ up to loadings of more than 20 wt % indeed fully enters the nanopores of the carbon support and that as a result the $NaAlH_4$ lacks long-range crystallinity. Hydrogen release and uptake of this nanocomposite is shown to be fundamentally different from that of bulk $NaAlH_4$ and $NaAlH_4$ mixed with nonporous carbon.

Experimental Section

High-purity porous carbon HSAG-500 (BET surface area 500 $m^2\ g^{-1}$, pore volume 0.65 $cm^3\ g^{-1}$, broad pore size distribution with a maximum around 2−3 nm, 90 wt % of the particles < 60 μm) and nonporous graphite KS-6 (20 $m^2\ g^{-1}$, 0.07 $cm^3\ g^{-1}$, 90 wt % of the particles < 5.8−7.1 μm) were obtained from Timcal Ltd., Switzerland. $NaAlH_4$ (>90%, Aldrich) was used as received as no impurities were detected with XRD and solid-state NMR. The observed chemical shift values for ^{23}Na and ^{27}Al concur with literature.[22] The carbon supports were dried at 500 °C for 3 h under an Ar flow before synthesis. Carbon support (80 wt %) and $NaAlH_4$ (20 wt %) were mixed in an Ar glovebox (Mbraun Labmaster I30, 2 ppm H_2O and < 1 ppm O_2) for 1 min in a mortar and transferred to an autoclave (Parr 4836). Melt infiltration was typically conducted by heating the sample under an H_2 atmosphere first to 170 °C (5 K min^{-1}, 10 min dwell time) and then to 200 °C (1 K min^{-1}, 15 min dwell time). The hydrogen pressure in the autoclave reached 200 bar at 200 °C. After cooling to room temperature, the pressure was released and the autoclave was transferred back to the glovebox, where the melt infiltrated sample was collected. XRD patterns were obtained with a Bruker AXS D8 Advance 120 machine (Co−K_α radiation) using an airtight sample holder. Nitrogen physisorption measurements were obtained at 77K using a Micromeritics ASAP 2020. BJH pore size distributions were calculated using the adsorption branch of the isotherm. Leaching of the melt infiltrated $NaAlH_4$ was done under reflux in a 1 M HCl solution (1 h) at 100 °C. ^{23}Na magic angle spinning (MAS) NMR spectra were recorded using a Chemagnetics Infinity 600 MHz spectrometer with a 2.5 mm HX MAS probe.[23] The single-pulse excitation spectra were obtained using a short hard pulse of 0.20 μs at a RF field strength of 200 kHz using sample spinning speeds of 10.2 kHz.

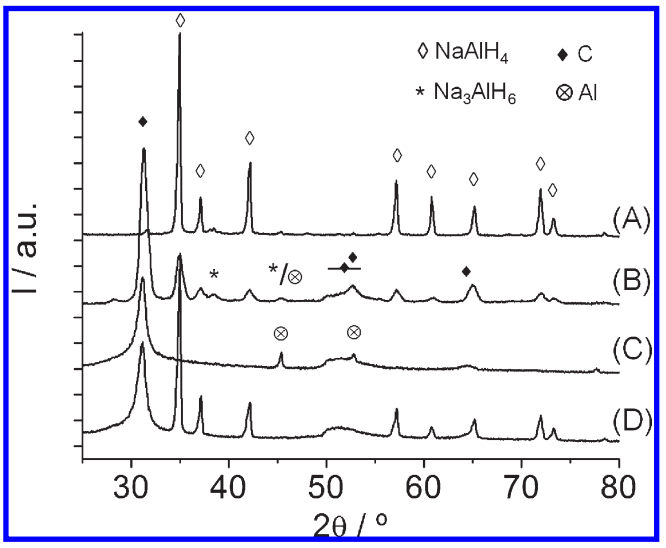

Figure 1. (A−C) XRD patterns of different samples after heat treatment at 200 °C under 200 bar H_2. (A) Pure $NaAlH_4$, (B) 20 wt % $NaAlH_4$ with nonporous graphite (mi20$NaAlH_4$/G), and (C) 20 wt % $NaAlH_4$ with porous carbon (mi20$NaAlH_4$/C). (D) A physical mixture of 20 wt % $NaAlH_4$ with porous carbon is added for comparison (20$NaAlH_4$/C). Note: The graphite support shows an additional carbon diffraction line at 52.5° that is absent for the porous carbon. The weak lines at 31 and 37° in curve A are the K_β lines of the intense diffraction lines at 35 and 42°.

High-pressure DSC (HP-DSC) measurements were obtained with an apparatus from Netzsch (DSC 204 HP Phoenix) at 120 bar H_2 operated in an Ar atmosphere glovebox.[24,25] This particular pressure was selected as it was the highest pressure experimentally available, and we wanted to avoid $NaAlH_4$ decomposition as much as possible. However, this implies that melting and equilibrium decomposition of $NaAlH_4$ can take place roughly at the same temperature, and kinetics will determine which process will dominate. Interpretation of the DSC results would be easier if measurements at significantly higher pressures than 120 bar H_2 would be possible. This was not the case at the time of writing, but recently the possibility of measuring up to pressures of 200 bar H_2 has been reported.[26]

Hydrogen release was studied by thermal programmed dehydrogenation under Ar flow (25 mL min^{-1}) using a Micromeritics AutoChem II equipped with a TCD detector. Rehydrogenation was performed in the autoclave (Parr 4836) at 150 °C with varying hydrogen pressures and dwell times.

Results and Discussion

Structural Characterization. Figure 1 shows the XRD patterns of various $NaAlH_4$/carbon samples that have previously been heated to 200 °C under H_2 pressure. For pure $NaAlH_4$ all diffraction lines corresponded to $NaAlH_4$ and proof recrystallization during cooling. This also implies that the decomposition of pure $NaAlH_4$ at 200 °C was effectively prevented by the high hydrogen pressure (curve A). Similar results were found when using

(22) Bogdanović, B.; Felderhoff, M.; Germann, M.; Hartel, M.; Pommerin, A.; Schuth, F.; Weidenthaler, C.; Zibrowius, B. *J. Alloys Compd.* **2003**, *350*, 246–255.
(23) Verkuijlen, M. H. W.; van Bentum, P. J. M.; van Eck, E. R. H.; Lohstroh, W.; Fichtner, M.; Kentgens, A. P. M. *J. Phys. Chem. C* **2009**, *113*, 15467–15472.
(24) Rongeat, C.; Llamas-Jansa, I.; Doppiu, S.; Deledda, S.; Borgschulte, A.; Schultz, L.; Gutfleisch, O. *J. Phys. Chem. B* **2007**, *111*, 13301–13306.
(25) Rongeat, C.; Llamas-Jansa, I.; Oswald, S.; Schultz, L.; Gutfleisch, O. *Acta Mater.* **2009**, *57*, 5563–5570.
(26) Mauron, Ph.; Bielman, M.; Bissig, V.; Remhof, A.; Züttel, A. *Rev. Sc. Instr.* **2009**, *80*, 095113.

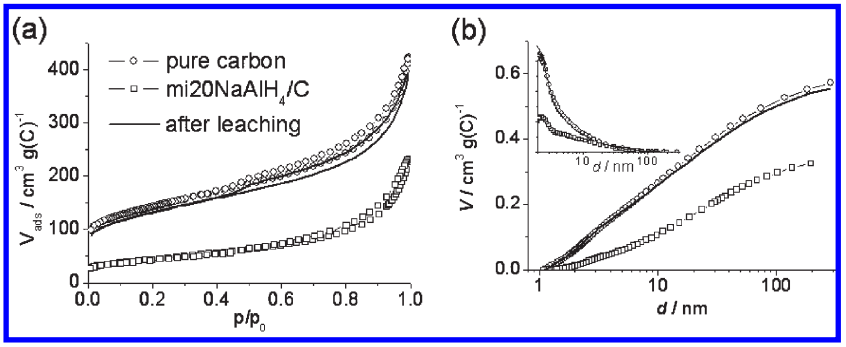

Figure 2. Results from nitrogen physisorption (77 K) comparing the porosity before (pure carbon, circles), after melt infiltration (mi20$NaAlH_4$/C, squares) and after leaching of $NaAlH_4$ (solid line). (a) Isotherms, (b) BJH cumulative pore volumes determined from the adsorption branch of the isotherms. The inset shows the corresponding pore size distribution (the unit of the *y*-axis is $cm^3\ g(C)^{-1}\ nm^{-1}$).

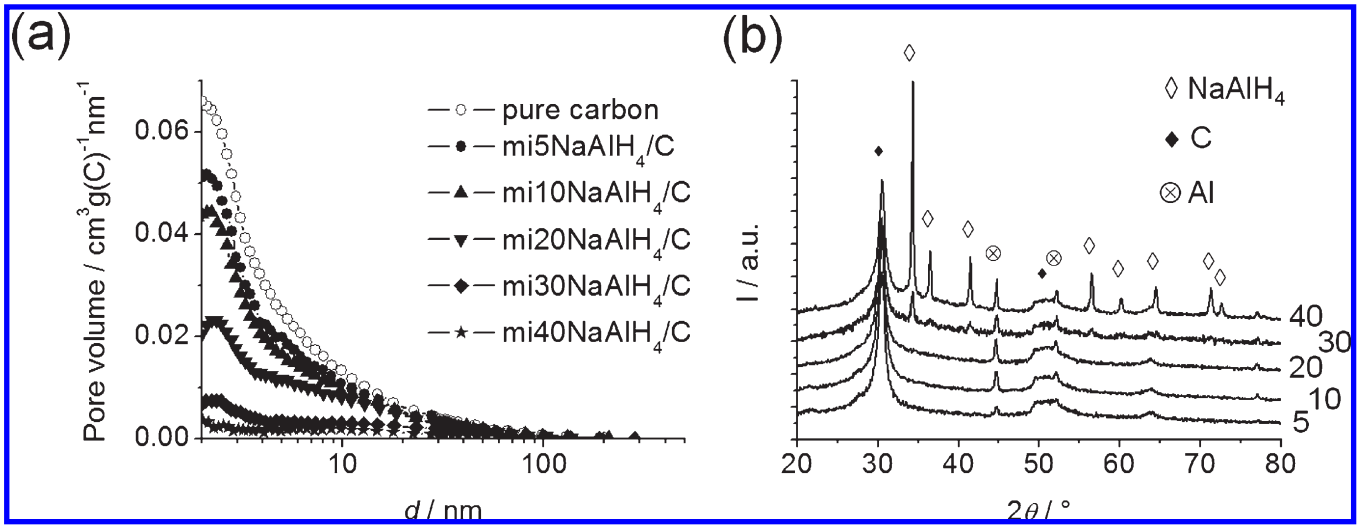

Figure 3. (a) Pore size distributions (BJH, adsorption branch) and (b) XRD patterns after melt infiltration for samples with different contents of $NaAlH_4$ 5−40 wt % (designated as miX$NaAlH_4$/C, where X denotes the $NaAlH_4$ content in wt %).

nonporous graphite as additive (curve B). However, in this case, the XRD pattern showed, besides the additional graphite diffraction lines, also some very weak features around $2\theta = 38$ and 45° that might originate from Na_3AlH_6 and Al. Hence graphite seems to promote the decomposition of liquid $NaAlH_4$, although the major fraction had not decomposed and recrystallized during cooling. Another interesting observation is that line broadening was observed (a crystallite size of 13 nm could be derived from the (112) diffraction line). This shows that there is interaction between nonporous graphite and $NaAlH_4$, hence that molten $NaAlH_4$ is able to wet a carbon surface, which was not a priori expected because of the low surface energy of carbon materials.[27]

No $NaAlH_4$ diffraction lines were found when using the porous carbon as support (curve C), showing that $NaAlH_4$ after melt infiltration lacks long-range crystallinity. This is in contrast to results reported for $NaAlH_4$ melt infiltrated into carbon aerogels where crystalline $NaAlH_4$ and its decomposition products were clearly identified with XRD, though the samples contained more $NaAlH_4$ (~50 wt %).[20] The presence of aluminum diffraction lines (crystallite size ~27 nm) shows that a minor amount of $NaAlH_4$ decomposed, albeit the high hydrogen pressure. No crystalline Na_3AlH_6 or NaH were detected. Compared to the physical mixture of $NaAlH_4$ and porous carbon (curve D), the carbon diffraction lines remain unchanged, indicating that the carbon structure was well-preserved during the melt infiltration process.

The pore filling of the nanocomposites was studied with nitrogen physisorption (Figure 2). For the pure carbon, the shape of the isotherm (Figure 2a) indicates a broad distribution of pores in the micro-, meso- and macropore range. After melt infiltration, a drastic loss in porosity was observed, indicating that the $NaAlH_4$ efficiently filled (or blocked) most of the pores upon melting. BET surface area and BJH total pore volume decreased from 500 to 156 $m^2\ g(C)^{-1}$ and from 0.57 to 0.32 $cm^3\ g(C)^{-1}$, respectively. The corresponding BJH cumulative pore volumes and pore size distributions are shown in Figure 2b. The melt infiltration leads to a loss in pore volume, in particular for the smaller pores. The theoretical volume $NaAlH_4$ added is 0.20 $cm^3\ g(C)^{-1}$ (assuming $\rho_{NaAlH4} = 1.24\ g\ cm^{-3}$). The total measured pore volume loss is 0.25 $cm^3\ g(C)^{-1}$ and 0.20 $cm^3\ g(C)^{-1}$ for pores ≤25 nm. Thus it can be assumed that, considering the results from

(27) Dujardin, E.; Ebbesen, T. W.; Hiura, H.; Tanigaki, K. *Science* **1994**, *265*, 1850–1852.

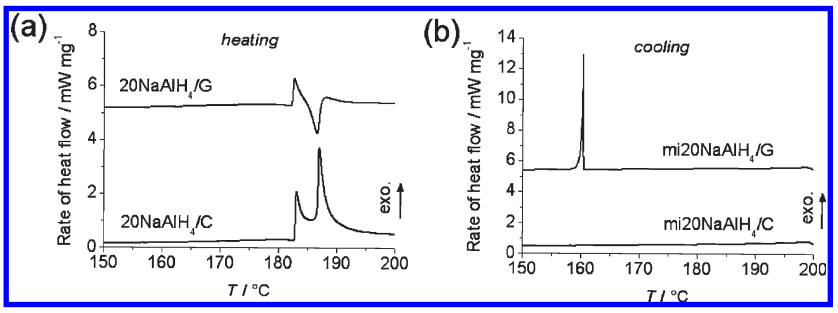

Figure 4. High-pressure DSC measurements (120 bar H_2, 5 K min^{-1}) starting from physical mixtures of $NaAlH_4$ with porous carbon (20NaAlH4/C) and nonporous graphite (20NaAlH4/G): (a) heating curves and (b) cooling curves. Note: The signals of 20NaAlH4/G and mi20NaAlH4/G are shifted by 5 mW mg^{-1} for better comparison.

XRD, the $NaAlH_4$ melt entered the pores of the carbon matrix and only minor pore blocking occurred.

Melt Infiltration Process. To study whether the carbon structure was affected by the melt infiltration, the porosity was redetermined after the $NaAlH_4$ had been leached. The pore volume corresponded well to the original carbon support, corroborating the findings from XRD that the carbon structure was well-preserved.

To follow the pore filling with increasing $NaAlH_4$ loading, a series of samples with $NaAlH_4$ contents from 5 to 40 wt % was prepared (Figure 3a). Considering the BJH total pore volume of 0.57 cm^3 g^{-1} of the carbon support, the maximum theoretical amount of $NaAlH_4$ that can enter the pores is 41.5 wt %. For the different $NaAlH_4$ loadings, the pore volume loss in the nanopore range is close to what would be expected. The difference between the expected and measured pore volume loss is similar for all samples up to 30 wt %, and typically around 0.06 cm^3 $g(C)^{-1}$. This indicates that a small fraction of the pore volume might be inaccessible for the $NaAlH_4$ melt, for instance because of the specific pore structure or the presence of impurities (which could lead to pore blocking due to reaction with the $NaAlH_4$).

For the sample containing 40 wt % $NaAlH_4$ (mi40$NaAlH_4$/C), the measured pore volume loss is slightly smaller than the calculated volume, indicating that not all $NaAlH_4$ entered the porous carbon matrix. This is as expected as this composition is close to the theoretical limit of 41.5 wt %, and hence one would expect some $NaAlH_4$ to be present outside the pores or in relatively large pores. This is in line with XRD observations (Figure 3b) where some crystalline $NaAlH_4$ was detected for loadings of 30 wt % and higher. Assuming ideal pore filling starting from the smallest pores for sample mi30$NaAlH_4$ (V_{NaAlH4} = 0.34 cm^3 $g(C)^{-1}$), pores up to 20 nm would be filled. However, experimentally we find that part of the pores of 5−20 nm are not filled, and that also part of the pore volume associated with pores larger than 20 nm is lost (see Figure S1 in the Supporting Information). The larger pores apparently allow crystallization of the $NaAlH_4$ upon cooling. For this reason, further experiments were conducted with samples containing 20 wt % $NaAlH_4$ (mi20$NaAlH_4$/C) to ensure that no crystalline $NaAlH_4$ is present. As the content of noncrystalline $NaAlH_4$ directly depends on the porosity of the carbon, it might be increased by using carbons with a higher pore volume in the low nanometer range. Interestingly, the intensity of the Al diffraction lines does not scale linearly with the $NaAlH_4$ content. This indicates that the minor decomposition of $NaAlH_4$ that is observed during the melt infiltration process is related to the contact with the carbon support. This speaks for a very efficient wetting of the support by the $NaAlH_4$ melt, i.e., the surface is already wetted to the maximum extent at low loadings.

An in situ study of the wetting and melt infiltration process was performed by DSC measurements under high hydrogen pressure (120 bar H_2) starting from physical mixtures of $NaAlH_4$ with porous carbon (20$NaAlH_4$/C) and graphite (20$NaAlH_4$/G).[27] Results are shown in Figure 4a. While heating up, the samples show both exothermic and endothermic contributions to the signal starting around the melting point of $NaAlH_4$ ($T \approx$ 181 °C). For both samples 20 wt % of $NaAlH_4$ is present in the physical mixture. We hence expect the same signal due to melting of the $NaAlH_4$ powder. This contributes an endothermic heat flow (ΔH_m = 23.2 kJ mol^{-1} or 28 kJ mol^{-1}).[28,29] A additional minor endothermic signal might also be present due to partial decomposition of liquid $NaAlH_4$ to Na_3AlH_6 (9 kJ mol^{-1}).[29] However, for both samples, a major exothermic contribution to the DSC signal is observed starting at the melting point of $NaAlH_4$. For the nonporous carbon, the exothermic heat flow is attributed to the wetting of the carbon surface area with molten $NaAlH_4$, even though we can not fully exclude a small contribution because of reactions with impurities of the high-purity carbons (e.g., oxygen containing terminating groups of the graphenes). This is a relatively rapid process, which is completed within about 2 min.

For the mixture with the porous carbon, the exothermic contribution is more than an order of magnitude larger than for the nonporous graphite sample. As the exothermic contribution is so much larger than the endothermic contribution, the profile seems to suggest that two separate exothermic contributions are present. However, as we are sure that the endothermic contribution due to the $NaAlH_4$ melting must be included, it is clear that the peak profile has to be explained by a relatively small and sharp

(28) Claudy, P.; Bonnetot, B.; Chahine, G.; Letoffe, J. M. *Thermochim. Acta* **1980**, *38*, 75–88.
(29) Bogdanović, B.; Brand, R. A.; Marjanovic, A.; Schwickardi, M.; Tolle, J. *J. Alloys Compd.* **2000**, *302*, 36–58.

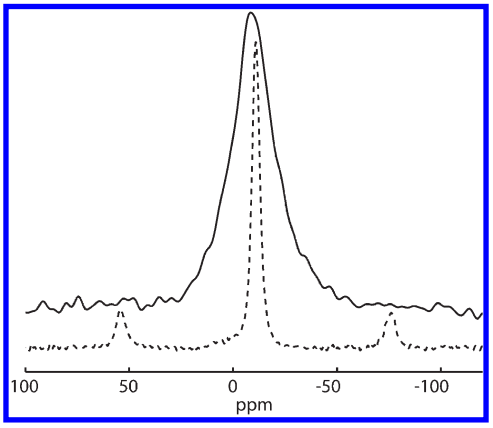

Figure 5. ^{23}Na NMR spectra before (20NaAlH$_4$/C, dotted line) and after melt infiltration (mi20NaAlH$_4$/C, solid line).

endothermic peak, superimposed on a broader and larger exothermic peak. Hence both for nonporous and for porous carbon, the peak shape is a result of the sum of both an endothermic and an exothermic contribution to the signal. However, in the case of the porous carbon, the process causing the exothermic signal (most probably the wetting of the carbon) takes somewhat longer time to complete (~3−4 min) than for the nonporous carbon (~1−2 min). How the peak shape can be deconvoluted into two contributions is illustrated in detail in the Supporting Information (Figure S3). Although a full quantitative analysis of the DSC is difficult because of the heat losses via the highly conductive hydrogen gas, it is clear that the exothermic signal roughly scales with the surface area of the carbons. The results strongly suggest that this exothermic process is a fingerprint of the infiltration of the carbon with molten NaAlH$_4$, hence eliminating the carbon/gas and NaAlH$_4$/gas surfaces and forming a low-energy NaAlH$_4$/C interface instead.

Additional information on the microstructure of the NaAlH$_4$ is obtained from the cooling curves after melt infiltration (Figure 4b). Interestingly, crystallization of NaAlH$_4$ upon cooling is only observed for 20NaAlH$_4$/G. It proves that in this case, a major fraction of the NaAlH$_4$ has not decomposed into Na$_3$AlH$_6$ under the given conditions. For 20NaAlH$_4$/C, no crystallization signal is observed at all. Clearly, the nanoconfinement and close contact with the carbon prevent crystallization. This phenomenon is known for other nanoconfined liquids, for instance, nickel nitrate aqueous solutions in silica pores, in which a glass phase rather than a crystalline phase is formed.[30,31] Upon a second cycling under the same conditions, no exothermic or endothermic signals were detected for the 20NaAlH$_4$/C nanocomposite, whereas the 20NaAlH$_4$/G sample showed repeated melting and recrystallization of the NaAlH$_4$.

(30) Findenegg, G. H.; Jahnert, S.; Akcakayiran, D.; Schreiber, A. *ChemPhysChem* **2008**, *9*, 2651–2659.
(31) Eggenhuisen, T. M.; van Steenbergen, M. J.; Talsma, H.; de Jongh, P. E.; de Jong, K. P. *J. Phys. Chem. C* **2009**, *113*, 16785–16791.
(32) Verkuijlen, M. H. W.; Gao, J.; Adelhelm, P.; van Bentum, P. J. M.; de Jongh, P. E.; Kentgens, A. P. M. *J. Phys. Chem. C* DOI: 10.1021/jp911228x.

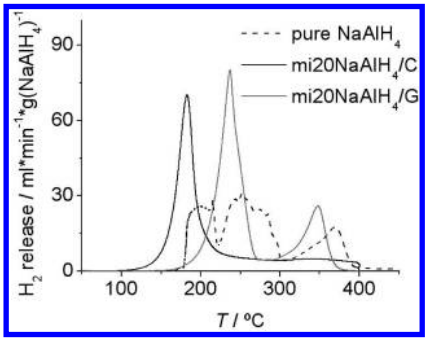

Figure 6. Thermal programmed dehydrogenation (Ar atmosphere, 25 mL min^{-1}, 5 K min^{-1}) of NaAlH$_4$ and after melt infiltration of porous carbon (mi20NaAlH4/C) and nonporous graphite (mi20NaAlH4/G).

Local Structure. As no long-range crystallinity was observed for the nanoconfined sample, few characterization techniques are available to study the local structure. One technique that gives full and quantitative information about the local surrounding of the atoms in these materials is solid-state NMR.

Figure 5 shows the ^{23}Na spectra before and after melt infiltration. Before melt infiltration the ^{23}Na spectrum shows a well-defined line at −11 ppm chemical shift with respect to a 0.1 M aqueous solution of NaCl, and spinning side bands at ±10.2 kHz, as expected for a well-crystallized (bulk) NaAlH$_4$ phase.[22] After melt infiltration (mi20NaAlH$_4$/C), the main line is clearly broadened and shifted downfield with respect to the resonance in the physical mixture. The broadening is attributed to a distribution in chemical shift and quadrupolar interaction parameters as a result of structural disorder indicating that the material is no longer crystalline. The shift of the resonance line to higher ppm values shows that, apart from the structural disorder, there are additional interactions that affect the effective shielding of the Na atoms in the melt infiltrated sample that are not present in the physical mixture. This can be caused by a multitude of effects such as susceptibility effects from the nearby carbon and coupling to conduction electrons in the carbon support. The exact identification and relative importance of the various possible interactions is beyond the scope of this paper.[32] From the fact that all Na atoms are affected in a similar way we can conclude, however, that the material must be very finely dispersed over the carbon support.

Hydrogen Release and Uptake. The combination of the experimental results clearly shows that a new NaAlH$_4$ phase is formed in the NaAlH$_4$/C nanocomposites, which lacks long-range order, and which is confined in such a way that every Na atom is close to carbon. An intriguing question is how this influences the hydrogen storage properties of the NaAlH$_4$, both in terms of thermodynamics and kinetics. Although a complete overview of the properties is outside the scope of this paper, Figure 6 compares the dehydrogenation of pure NaAlH$_4$ and the melt infiltrated samples miNaAlH$_4$/C and miNaAlH$_4$/G.

As expected, pure NaAlH$_4$ shows a dehydrogenation profile with several steps starting from around its melting point. The first two steps between 180 and 300 °C

correspond to the decomposition of $NaAlH_4$ via Na_3AlH_6 to NaH.[28] However, it should be noted that the measurement of pure $NaAlH_4$ is difficult because its melting can partly block the sample holder and sudden gas evolution during decomposition leads to a nonsteady gas flow. The peak with a maximum release rate at 370 °C is due to the decomposition of NaH. mi20$NaAlH_4$/G shows a clearly different dehydrogenation profile with a first maximum at 235 °C and the decomposition of NaH at 350 °C. Hydrogen release starts already from 160 °C, but the average hydrogen release temperature associated with the transition from $NaAlH_4$ to NaH is comparable to the average release temperature of the first two decomposition steps in bulk $NaAlH_4$. The nanosized $NaAlH_4$ (mi20$NaAlH_4$/C) shows a significantly improved dehydrogenation behavior with H_2 release starting already around 110 °C, reaching its maximum rate around 180 °C. A slow further loss of hydrogen is observed for temperatures above 200 °C. Pure $NaAlH_4$ and mi20$NaAlH_4$/G released hydrogen close to their theoretical capacity of 7.4 wt % $g(NaAlH_4)^{-1}$. A slightly lower value of 6.3 wt % was found for mi20$NaAlH_4$/C. This in line with the results from XRD showing that a minor amount of the $NaAlH_4$ had already decomposed during the synthesis. However, the fact that the hydrogen yields are significantly higher than 5.5 wt % proves that also the decomposition of NaH is facilitated due to the presence of carbon, as has been also reported recently.[10] Rehydrogenation of mi20$NaAlH_4$/C was found to start already under very mild conditions, yielding 2.4 wt % H per gram $NaAlH_4$ when rehydrogenating at 24 bar (150 °C, 3 h) and 3.3 wt % at 55 bar (150 °C, 15 h) even though no metal-based catalyst had been added to the system. An improvement in the hydrogen storage properties due to high dispersion and close contact with carbon is discussed in detail elsewhere.[33] Furthermore, no crystalline $NaAlH_4$ was detected with XRD after rehydrogenation (see Figure S2 in the Supporting Information), evidencing that the reversible interaction of $NaAlH_4$ and its decomposition products with H_2 occurs on the nanoscale. However, crystalline Al is detected after rehydrogenation (see Figure S2 in the Supporting Information), which might be present outside the nanopores of the carbon, and hence limit reversibility of these systems. In the bulk phase, rehydrogenation of $NaAlH_4$ under these mild conditions is not possible because of the phase segregation of the decomposition products. This is demonstrated by the very limited degree of rehydrogenation of mi20$NaAlH_4$/G, which yielded only 0.16 wt % under the same conditions (24 bar, 150 °C, 3 h).

(33) Gao, J.; Adelhelm, P.; Verkuijlen, M. H. W.; Rongeat, C.; Herrich, M.; van Bentum, P. J. M.; Gutfleisch, O.; de Jong, K. P.; Kentgens, A. P. M.; de Jongh, P. E. *J. Phys. Chem. C* DOI: 10.1021/jp910511g.

Conclusion

The $NaAlH_4$ melt infiltration of porous carbon is an effective and simple method to synthesize highly loaded $NaAlH_4$/carbon nanocomposites. Wetting of the carbon with the molten $NaAlH_4$ is observed when following the process in situ with HP-DSC experiments. Combined with N_2 physisorption results, it becomes clear that the majority of the pore volume of a nanoporous carbon can be filled with $NaAlH_4$ within a few minutes. Due to the nanoconfinement, the structure of the resulting $NaAlH_4$ phase is clearly different from bulk crystalline $NaAlH_4$. It lacks crystallinity, and does not show melting and solidification as is found for bulk $NaAlH_4$. ^{23}Na NMR characterization shows that the local surrounding of the Na atoms is clearly heterogeneous and suggests intimate contact between all $NaAlH_4$ and the nanoporous carbon, at least for loadings of 20 wt %. The carbon structure itself is preserved during the synthesis. The nanosized $NaAlH_4$ reversibly releases and takes up H_2 under very mild conditions which can be at least partially attributed to reduced diffusion path lengths and the presence of the carbon support. Although loadings up to 20−30 wt % of nanoconfined $NaAlH_4$ can already be obtained, a further increase could be expected by optimizing the carbon pore structure.

Acknowledgment. We thank dr. A. Brinkmann and dr. ERH van Eck of the Solid-State NMR Facility for Advanced Materials Science for support and discussions (Nijmegen), NWO for financial support of this facility, and Andy Beale (Utrecht University) for carefully checking the language of the manuscript. We are grateful to Timcal Ltd., Switzerland, for providing the High Surface Area Graphite. NWO-ACTS/Vidi is acknowledged for financial support of this project, as well as the EU-RTN project (COSY) and HGF project (FuncHy).

Supporting Information Available: (BJH cumulative pore volumes of pure carbon and mi30$NaAlH_4$/C; XRD pattern after rehydrogenation of mi20NaAlH4/C; illustration of how the DSC peak shape can be deconvoluted into one endothermic and one exothermic component. This information is available free of charge via the Internet at http://pubs.acs.org/.